

Mechanical and Sliding Wear Performance of ZA27-Gr Alloy Composites for Bearing Applications: Analysis Using Preference Selection Index Method



Ashiwani Kumar and Mukesh Kumar

Abstract In this chapter, the sliding wear and mechanical performance of Gr-ZA-27 alloy composites are investigated following ASTM standards. Taguchi methodology is used in designing sliding wear experiments, and the same methodology is used for parametric optimization. In order to comprehend the associated wear mechanisms responsible for surface damage, surface micrograph studies employing scanning electron microscopy (SEM) are conducted. Furthermore, the rank of designed compositions is evaluated using Preference Selection Index (PSI), and decision-making technique. The physical and mechanical characteristics of alloy composites with reinforcement are found to be improved, including void content (1.33–2.50), hardness (107–171 HV), compressive strength (406–496 MPa), flexural strength (300–490 MPa), tensile strength (290–428 MPa), impact strength (22.76–64 J), and sliding wear performance. It is found that the AGr-6 alloy composite showed to optimize the overall physical, mechanical, and sliding wear performance. The evaluation of performance data using the PSI and decision-making tool reveals that the order of material composition that optimizes the required performance is AGr-6 > AGr-4 > AGr-2 > AGr-0. As both decisions are attained, decision-making technologies like PSI can be applied to these challenges of material selection.

Keywords ZA-27 alloy · Graphite powder · Dry sliding wear · Mechanical properties · Preference Selection Index method (PSI)

A. Kumar (✉)

Department of Mechanical Engineering, Feroze Gandhi Institute of Engineering and Technology, Raebareli 229316, U.P., India
e-mail: ashi15031985@gmail.com

M. Kumar

Department of Mechanical Engineering, Malaviya National Institute of Technology, Jaipur 302017, Rajasthan, India

1 Introduction

ZA-27 alloy is a typical monolithic material that is employed in automobile company. This material is used for bearing material application and it shows outstanding characterizations such as fluidity, castability, mechanical properties and wear resistance. Tribological-based properties are being opted into consideration for different applications such as piston material, cylinder and aerospace/automobile industry [1, 2]. Raju et al. [3] investigated the mechanical characteristics of Silicon-carbide (SiC)-ZA27 alloy. It was found that the increase in weight percentage of reinforcement improves the mechanical properties (such as hardness, tensile strength, impact strength, and compressive strength) of composites. The improvement in mechanical properties is due to the effect of ceramic reinforced based alloy matrix. Dalmis et al. [4] investigated the impact of inclusion of Gr nano powder particles on the mechanical and physical characterization of ZA-27 alloy composites. It is found that the hardness and tensile strength diminish as the filler content increases. The ductility of composite increases with the increases in Gr content. It may be attributed to the improvement in mechanical characteristics because of the strong bonding between matrix and reinforcement. Ranganath et al. [5] studied the mechanical properties and fractography characteristics of TiO₂ reinforced ZA27 alloy based composite. It was observed that mechanical properties such as Young's modulus, ultimate tensile strength, yield strength, and hardness increase with the increase in TiO₂ content. Sharma et al. [6] investigated the influence of short glass fibres on the mechanical properties of cast ZA-27 alloy composites. It was found that the mechanical characteristics such as tensile strength, hardness, and Young's modulus improve with the increase in filler content. Alaneme et al. [7] studied the mechanical and wear behaviour performance of Steel chips reinforced ZA27 alloy based composites. It was found that increasing the weight percentage of reinforcement improved the composites' hardness and wear resistance. Girisha et al. [8] and Baradeswaran et al. [9] examined the effects of composites reinforced with graphite and the ZA-27 alloy. It was found that the increase in filler content resulted in better mechanical and tribological qualities. Kumar and Kumar [10] evaluated the mechanical and sliding wear performance improvement as the filler content rises. Similar findings are published by Ashiwani and Mukesh [11] and Kumar et al. [12]. It is noticed that the impendence of Gr reinforced ZA27 alloy composite indicated increased wear resistance of investigated composites with the increasing Gr content. In their study of the impact of AA7075SiC/Marble Dust/Graphite Hybrid alloy composites on their mechanical and sliding performance, Kumar et al. [13] discovered that the performance of the mechanical and sliding wear improved as the filler content increased. Using the PSI approach, Kumar et al. [14] determined the ranking performance of the composite by analysing the effects of Al₂O₃/SiC on the mechanical and wear performance of the AA2024 alloy. For the mechanical and sliding performance of particle filled alloy composite, similar results have been reported by other researchers [15–17]. The unit cost approach and digital logic method, which are used to analyze the performance of materials, were covered by Maleque et al. [18]. Similar outcomes have been reported

by Maniya [19] and Kumar [20], who proposed utilizing the presence selection index approach to choose the content and rank it in terms of preference. For the purpose of choosing materials for certain applications, design engineers can benefit from this strategy.

The mechanical and sliding wear performance of graphite-filled ZA27 alloy composites is covered in this chapter. Using decision-making tools and PSI techniques, the ranking of manufactured composite materials was carried out. Decision-making technologies such as PSI could be applied in such material selection issues because both decisions are tuned.

2 Materials and Methodology

2.1 Materials, Design and Fabrication Procedure

The ZA-27 alloy was obtained from Bharat Aerospace Metals in Mumbai, India, as rods with the following composition: aluminium (25–28 wt.%), Copper (1.0–2.5 wt.%), Magnesium (0.01–0.02 wt.%), Iron (~0.075 wt.%), lead (~0.006 wt.%), Tin (~0.003 wt.%), and the rest is Zinc wt.%. While Graphite particulates (99 μm) were procured from Savita Scientific Pvt. Ltd. Jaipur. The four alloy compositions (AGr-0, AGr-2, AGr-4, and AGr-6) were fabricated using a high vacuum casting method.

The precise fabrication process is as follows:

- The ZA-27 metal long rods that were measured out were cleaned and cut into little pieces. The tiny bits were melted using a high vacuum induction furnace inside a graphite crucible. The amount that had melted was maintained at 870°C for 20 minutes. After that, the temperature was decreased to between 430 and 660 °C (the alloy's solidus and liquid temperature). The quantities of reinforcements were separately preheated at 300 °C for 3 h.
- Magnesium powder (2 wt%) was added to the molten metal in order to increase the Gr phase's wettability.
- A completely automatic magnetic stirrer (made of stainless steel; speed: 280 rpm; time: 10 min.) was employed to ensure that the graphite phase was added uniformly to the melt.
- The mixture was placed into a stationary 150 × 90 × 10 mm³ cast iron mould and allowed to solidify to 30 °C in air for at least 45 min.
- The specimens were cut using a wire Electric Discharge Machine (EDM) in accordance with ASTM standards, and their dimensions were then polished with sandpaper in various sizes.

2.2 Physical and Mechanical Characterization

The physical characteristics of the Gr-reinforced ZA-27 alloy composite, including its actual density, theoretical density and vacancy fraction are investigated. The void fraction was determined using the water displacement method utilising the Archimedes principle approach and the ASTM D792 standard, and the experimental density of planned composite specimens was calculated. Using Eq. 1 [21], it was possible to calculate density of samples by using the rule of mixture:

$$\rho_c = \frac{1}{\left(\frac{W_p}{\rho_p}\right) + \left(\frac{W_m}{\rho_m}\right)} \quad (1)$$

where W stands for the weight fraction, p for the phase of particles and m for the phase of the matrix. ρ_p and ρ_m represent densities of the particulates and matrix phases respectively.

Using Eq. 2 [17], the voids fraction of planned composite samples was calculated.

$$\text{Void fraction} = \frac{\text{Theoretical } (\rho_t) - \text{Experimental } (\rho_e)}{\text{Theoretical } (\rho_t)} \quad (2)$$

The proposed composite of hardness was evaluated by using hardness tester (ASTM E92 standard; Walter Uhl testing tester). Specimens were tested for hardness under a 180 g load for 15 s. Each sample indentation is held using a diamond indenter. Vickers hardness was calculated using Eq. 3 using the average of the five measurements taken five times for each specimen of the specified composite.

$$\text{HV} = 1.854 \frac{L}{D} \quad (3)$$

where D is the indenter's diagonal dimension (in mm) and L is the applied load (in g).

The UTM equipment (ASTM: E-8) was used to performed tensile tests on composite specimens while parameters such as the specimen's (flat shape) dimensions of $160 \times 10 \times 10 \text{ mm}^3$ and the cross-head speed of 2 mm/s were chosen. An ASTM E-290 universal testing machine was used to conduct a flexural experiment on composite samples. Selected parameters, including (specimen dimension = $50 \times 10 \times 10 \text{ mm}^3$; span length = 40 mm; cross-head speed = 2 m/s), were carried out in accordance with the (ASTM E- 290) standard. Using Eq. 4 [12], the flexural strength (F) was calculated.

$$F = \frac{3PL}{2bt^2} \quad (4)$$

where P is the load (kg), b is the specimen's width (mm), t is the sample's thickness (mm) and L is the sample's span length (mm).

On impact tester equipment (executed in accordance with ASTM E-23) the composite specimen (impact strength) was completed, and the machine settings were chosen as follows: specimen size = $64 \times 12.8 \times 3.2 \text{ mm}^3$; depth of notch = 10.2 mm. The ASTM E9-09 compression tester was used to determine the compressive strength of the composite specimen, and the compression test on UTM was carried out with the following parameters: specimen size = $10 \times 10 \times 10 \text{ mm}^3$, span length = 0.5 mm, speed = 2 m/s.

2.3 Multi-Specimen Dry Sliding Wear Tribo-Meter

Multi-specimen Tribo-tester apparatus was used to measure the friction and tribological performance. Figure 1 presents an image of this apparatus, with required specifications of a revolving disc made of 62 HRC hardened steel, a specimen with dimensions of $14 \times 9 \times 10 \text{ mm}^3$, a load given to a fixed specimen in a vertical direction, and other details. A fixed load of 20 N and sliding velocities of 1, 1.25, 1.5, and 1.75 m/s were chosen as the steady state wear performance condition parameters. On the Tribo-tester, the analysis of sliding behaviour (five repetitions of 700 m each; constant disc track diameter = 40 mm) was done, and the composite wear rate was also acquired. Every test result was measured in an environmental setting. Following this, samples were taken using various sizes of abrasive paper, such as (200–600 grit), for a brief period of time to remove debris particles and collected material, which were taken for sampling, and regularly cleaned samples with alcohol.

The experimental design employed the Taguchi orthogonal array, with the parameters and their levels stated in Table 1. Each sample was then cleaned. Prior to this, the pin-type sample was weighed using an Electronic Balance Machine (EBM) with a $1 \times$

Fig. 1 Multi-specimen tribometer (Model: TR-705 of Ducom Instruments)



10⁻³ mg precision. The equipment was used to gather and analyse the experimentally recorded value on wear rate and coefficient of friction. As a result, Table 2 includes the experimental specific wear rate numerical values. Following Eq. 5 led to the development of a novel alloy composite with particular wear rates (Ws) [23].

$$W_s = \frac{\Delta m}{\rho \times v_s \times t \times f_n} \tag{5}$$

where Δm = mass loss (g); density (ρ); the sliding velocity (v_s); the test duration (t); and the normal load (f_n).

Table 1 Working range of selected parameters

Control parameter	Level					Units
	I	II	III	IV		
Normal load (A)	10	20	30	40		N
Filler content (B)	0	2	4	6		%
Sliding velocity (C)	1	1.25	1.50	1.75		m/s
Sliding distance (D)	700	1400	2100	2800		M

Table 2 Experimental response table for L16 orthogonal array layout

Sample number	Normal load (N)	Filler content (wt.%)	Sliding distance (m)	Sliding velocity (m/s)	Specific wear rate (mm ³ /Nm)	S/N ratio (dB)
1	10	0	700	1	0.000188300	74.5030
2	10	2	1400	1.25	0.000193836	74.2513
3	10	4	2100	1.5	0.000265287	71.5257
4	10	6	2800	1.75	0.000163827	75.7123
5	20	0	1400	1.5	0.000337371	69.4378
6	20	2	700	1.75	0.000371519	68.6004
7	20	4	2800	1	0.000360625	68.8589
8	20	6	2100	1.25	0.000196592	74.1287
9	30	0	2100	1.75	0.000118559	78.5213
10	30	2	2800	1.5	0.000191144	74.3728
11	30	4	700	1.25	6.63218E-05	83.5669
12	30	6	1400	1	8.19135E-05	81.7329
13	40	0	2800	1.25	0.000125534	78.0248
14	40	2	2100	1	0.000115763	78.7286
15	40	4	1400	1.75	0.000116063	78.7061
16	40	6	700	1.5	0.00018021	74.8844

2.4 Experimental Design and Surface Morphology Studies

A useful tool for optimizing a variety of control parameters, including the load, sliding velocity, filler content and sliding distance, as well as an examination of the sliding wear behaviour of specified composites, was the thorough Taguchi design technique. The signal-to-noise (S/N) ratio derived from the experimental data of proposed composite utilizing (Eq. 6) represents the performance qualities in this approach. So, using the lower-the-better (LB) features approach, the wear rate performance was examined. The various input parameters are shown in Table 1 together with their quantified values.

The experiment's Taguchi design (L16 orthogonal array) used the wear rate as the output parameter. In terms of Eq. 6, the S/N ratio with the lower-the-best characteristic is expressed. Analysis of variance (ANOVA) is also carried out in order to rank the relevance of input characteristics on output performance (such as Wear rate).

$$\frac{S}{N} = -10 \log \frac{1}{N} \sum Y^2 \quad (6)$$

where N = number of observations, and Y = observed data measurement.

The behaviour of a SEM micrograph of worn-out surfaces is examined using a field emission scanning electron microscope (FESEM; FEI Nova Nano SEM 450, USA) in order to comprehend the wear process of developed composite.

2.5 Preference Selection Index Method Algorithm

Design engineers can use the PSI technique as a methodical, scientific methodology or instrument to choose the best material for a certain application. When there is a conflict in assessing relative significance of qualities, which is the PSI method's weakness, this methodology can be helpful. The next phases represent the precise PSI computing processes [24–28].

Step 1: The structure of decision problem: For PSI, data entry is necessary, for example, to compile all material choices and selection criteria for a certain application. This strategy aids in determining the objective. According to some academics, the typical decision-making problem's hierarchical structure makes it possible to understand the issue clearly. The primary goal should be at the top of the hierarchy, followed by the ranking criteria for evaluation and finally the alternatives/options. Thus, Fig. 2 [29, 30] depicts the hierarchical structure of the problem.

Step 2: Formulating the decision matrix: A multi-alternative (say m-alternatives) and multi-criteria (say n-criteria) formulation of the issue is used. Additionally, the model also expresses the decision matrix's product (for example, the matrix D of order $m \times n$ order).

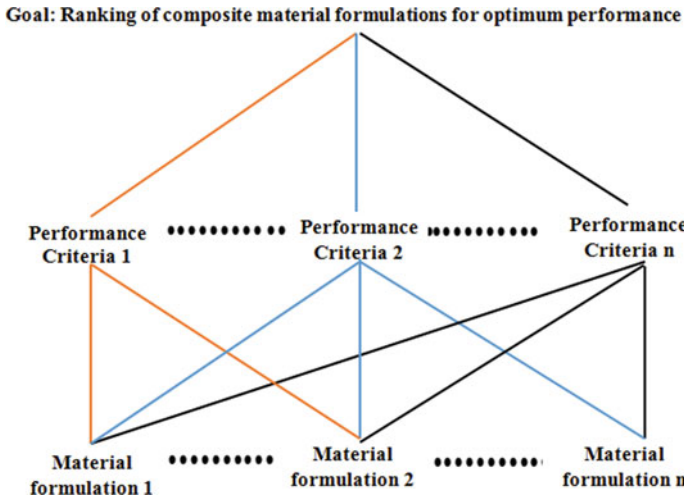


Fig. 2 Hierarchical structure of the problem

$$\begin{matrix}
 C_1 & C_2 & \cdots & C_n \\
 A_1 & \begin{bmatrix} p_{11} & p_{12} & \cdots & p_{1n} \end{bmatrix} \\
 A_2 & \begin{bmatrix} p_{21} & p_{22} & \cdots & p_{2n} \end{bmatrix} \\
 \vdots & \begin{bmatrix} \vdots & \vdots & \ddots & \vdots \end{bmatrix} \\
 A_m & \begin{bmatrix} p_{m1} & p_{m2} & \cdots & p_{mn} \end{bmatrix}
 \end{matrix}
 \quad \text{where } C_1, C_2, \dots, C_n \text{ are the } n\text{-criteria and } A_1, A_2, \dots, A_m \text{ are the } m\text{-alternatives}$$

The element p_{ij} is the performance value of the i th alternative (A_i) with respect to the j th attribute (C_j), where $i = 1, 2, \dots, m$ and $j = 1, 2, \dots, n$.

Step 3: Normalization of the decision matrix: Normalization is the process of transforming the decisive data range of 0 to 1 and is needed in order to transform performance rating with the various data measurement units into a compatible unit. In order to compute all criteria in unitless, and to facilitate inter-attribute comparisons, the above matrix entries are normalized (using the principle below). Thus, find out normalized matrix is R_{ij} .

(i) If the expectation is *larger-the-better*, then the performance of the original attribute can be normalized as follows: (Eq. 7).

$$R_{ij} = \frac{x_{ij}}{x_j^{max}} \tag{7}$$

(ii) If the expectation is *smaller-the-better*, then the performance of the original attribute can be normalized as follows: (Eq. 8).

$$R_{ij} = \frac{x_j^{min}}{x_{ij}} \tag{8}$$

where x_{ij} are the measures of the attribute ($i = 1, 2, 3, \dots, m$, and $j = 1, 2, 3, \dots, n$).

Step 4: Computation of preference variation value (PV_j): The normalized matrix R_{ij} , is used to measure preference variation value (PV_j) for each criterion with the concept of sample variance using the following Eq. 9:

$$PV_j = \sum_{i=1}^N (R_{ij} - R_j)^2 \tag{9}$$

where R_j is the mean of normalized values of criteria j i.e. $R_j = \frac{1}{n} \sum_{i=1}^N R_{ij}$

Step 5: Computation of overall preference value (ψ_j): The overall preference value (ψ_j) of every criterion is calculated using the following 10:

$$\Psi_j = \frac{\Phi_j}{\sum_{j=1}^n \Phi_j} \tag{10}$$

where $\Phi_j = 1 - \sum PV_j$, is the deviation in the preference value of each criterion. For consistency, the sum of overall preference values for all the criteria should be unity i.e. $\sum \Psi_j = 1$.

Step 6: Computation of Preference Selection Index (I_i): The preference selection index (I_i) for each alternative is measured using the following Eq. 11:

$$I_i = \sum_{j=1}^n (R_{ij} \times \Psi_j) \tag{11}$$

Step 7: The computed values of preference selection index (I_i): The computed values of preference selection index (I_i) are used to rank the alternatives according to their descending order, i.e. highest to lowest I_i value is used to rank the alternatives from first to last and then making related interpretations or recommendations.

3 Result and Discussion

3.1 Physical and Mechanical Characteristics

3.1.1 Effect of Filler on Voids Content and Density of developed Composite

Figure 3 shows the impact of graphite on the amount of voids in a Zinc Aluminium (ZA-27) alloy composite filled with 0, 2, 4, and 6 wt% filler, respectively. For the planned composites of both theoretical and experimental densities, the results of the void fraction experiment are obtained. While the void fraction of the intended

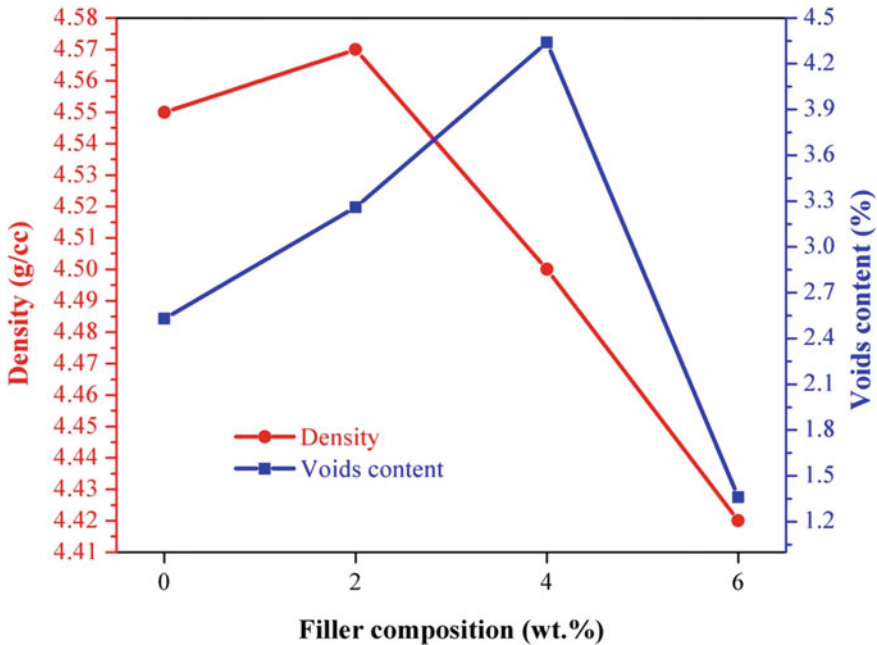


Fig. 3 Effect of Gr on the density and the voids content of alloy composite

alloy composites is gradually improving due to an increase in reinforcement, the void fraction of the 6 wt.% Gr-ZA-27 alloy composite is on the decline. Due to the perfect blending of the reinforcement and the composite matrix, the greater weight percentage of void contents appears to be minor and may rely on the shape and size of the individual particle.

The change in density and void content with rise in graphite content of filled ZA-27 alloy composite was presented in Fig. 3. It has been noticed that increasing the graphite component causes the density of the designed composite to drop. The added 2 weight per cent Gr-reinforced ZA-27 alloy composite has a density of 4.42 g/cc, compared to the 4.55 g/cc of the pure alloy composite. A further addition is a 4.30 g/cc (4 wt.%) gr powder. Adding 6.0% Gr powder again reduces the base alloy's density by 3.6% to 4.36 g/cc. It should be observed that the composite's density falls as a result of Gr particles' decreased weight relative to the base alloy. With an increase in rice/Sic powder particle, the density of the composite falls [12, 31].

3.1.2 Effect of Filler on Hardness

Figure 4 depicts the effect of graphite on the hardness of the designed alloy composites. It has been found that adding more reinforcement increases the hardness of planned alloy composites. When compared to unfilled alloy composite, the ZA 27-6

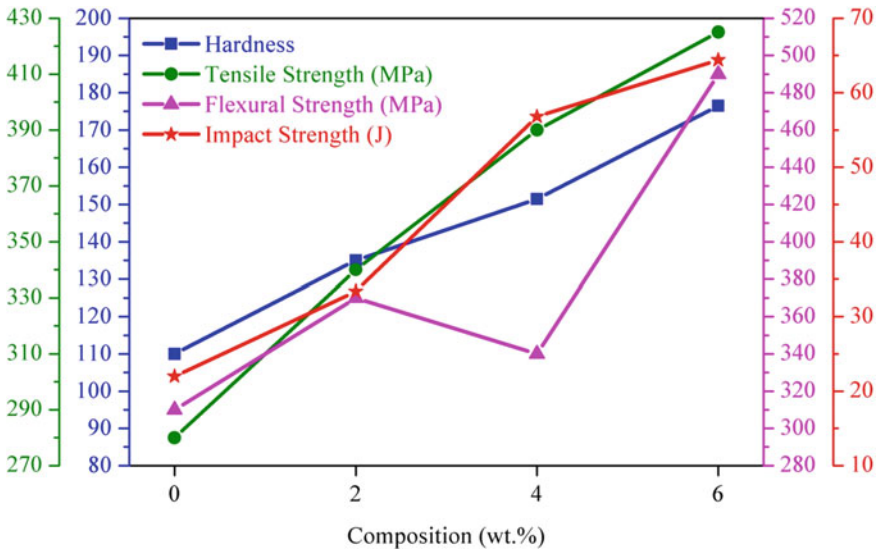


Fig. 4 Effect of Gr on the mechanical characteristics of alloy composite

wt.% Gr alloy composite exhibits greater hardness. The graph reveals that the clean alloy composite has a hardness of 107 HV. Hardness of alloy composite increases (135 HV) with the addition of 2 weight per cent graphite powder. Once more, adding 4 wt.% and 6 wt.% of graphite powder to a pristine alloy composite results in an increase in hardness to 157 HV and 171 HV, respectively. Similar results are reported by Dali et al. [32], who found that incorrectly mixed graphite reinforced with matrix caused the graphite-reinforced ZA-27 alloy composites to grow with increasing Gr content. According to Sharma et al. [33], enhancements in addition to graphite-reinforced particles boost the composite’s hardness by enhancing the bonding strength and load-bearing capability of the matrix and reinforcement. According to Rajmohan et al. [34], adding mica boosted the composite’s hardness, which enhanced the produced composite’s mechanical capabilities.

3.1.3 Effect of Filler on Flexural Strength

The change in flexural strength on the graphite-filled ZA-27 alloy composite is depicted in Fig. 4. It has been found that adding an additional 2 wt.% of graphite reinforcement increased the flexural strength of the specified specimen. The flexural strength was then decreased by the inclusion of an additional 2 wt% Gr content. The trend of increased flexural strength was maintained by increasing the graphite content to 4 and 6 wt.%. As a result, this may be the proper particle dispersion, and the right casting procedure is what created the strongest binding. Therefore, increasing the graphite concentration increases the flexural strength of specified specimens. As

the amount of distortion of the material reduces, an increase in ductility may be the cause of the rise in flexural strength. Therefore, this is the interfacial bonding strength between the matrix and the reinforcement that is the strongest. These findings are in perfect accordance with other research in this field [35].

3.1.4 Effect of Filler on Tensile Strength

Figure 4 shows the effect of graphite particles on the tensile strength of an alloy composite made of zinc and aluminium (ZA-27). By use of the software-based computerized UTM Machine, the tensile strength of the specified composite was computed. It has been found that increasing the graphite content produces better results in terms of tensile strength. The improvement in composite's hardness and strength is what causes the planned specimens' increased tensile strength, and the addition of graphite increases tensile strength while reducing elongation [36]. The intended specimen is found to have a tensile strength of 290 MPa at 0% Gr reinforcement. The designed specimen has a tensile strength of 340 MPa after being further strengthened with a 2 wt.% Gr component. Tensile strengths of 395 and 428 MPa are obtained by increasing the Gr content in the composite sample to 4 and 6 wt.%, respectively. Similar findings reported by Ramnath et al. [22] found that the base alloy matrix and Gr particles had a strong connection, increasing the tensile strength of the planned composite specimen. It should be emphasized that the base material's matrix and filler both significantly contribute to the composite's improved specimen strength.

3.1.5 Effect of Filler on Impact Strength

Figure 4 illustrates graphite particles effect on the impact resistance of the ZA-27 alloy composite. The impact strength of the composite obtained by the Izod experiment is observed to rise as the weight percentage of graphite is increased. The intended composite specimen has an impact strength of 23.56 J at 0% Gr content. Once more, increasing the reinforcement content to 2, 4, and 6 wt.% raises the composite's impact strength to 33.5, 58.5, and 64 J, respectively. When compared to base alloy matrix, the developed composite's maximum impact strength at 6 wt.% Gr is lower. Similar conclusions made by Ozden et al. demonstrated that better resistance ability was the reason why impact strength increased. As the particle size and hot extrusion ratio are increased, the composite's impact strength somewhat improves. Due to temperature's influence, the impact strength is also increased [32].

3.1.6 Effect of Filler on Compressive Strength

The effect of graphite powder filler on compressive strength of ZA-27 alloy composite is depicted in Fig.5. It is found from the graph that the compressive strength of filled

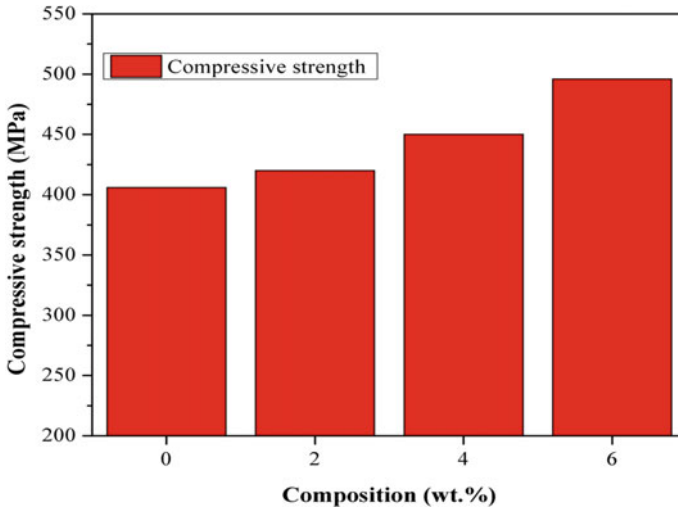


Fig. 5 Influence of Gr on the compressive strength of alloy composite

designed composite is larger than that of unfilled alloy composite. The compressive strength of designed specimen increases with the increase of graphite content. The compressive strength of unfilled alloy composite (at 0 wt. % Gr content) is 406 MPa. Addition of Gr content to 2 wt.% and 4 wt.% increases the compressive strength to 420 MPa and 450 MPa respectively. The higher compressive strength value of designed composite is 496 MPa at 6 wt.% Gr content.

The compressive strength of designed composite which gradually increases with the increase in graphite content may cause the growth of hard ceramic particles that stop the movement of modified crack and dislocation levels as outcome result of size of Gr network. Also, the strengthening mechanism of dispersion is likely to be continued even at higher temperature [12].

3.2 Steady State-Specific Wear Condition

Figure 6 displays a plot of the specific wear rate of an unfilled alloy and its specified composites with varying graphite contents against sliding velocity. The specific wear rate reduces as the sliding velocity increases, as shown in Fig. 6. The figure also demonstrates the specific wear rate of the designed composite drops as the graphite content is increased; it is discovered to be lower at a graphite content of 6 wt.% than that of other designed composites with different graphite content percentages. Therefore, the material with 0% composite has the highest specific wear rate. The production of the lubricating tribo-layer, porosity, fissures, and the abrasion process are few examples of possible causes for the decrease in specific wear rate with the

addition of graphite content [8]. That is, the addition of the graphite reinforcement may serve as a thick layer of solid lubricant between the mating surfaces. The precise wear rate behaviour is in line with the patterns noticed by a small number of academics and materialists [37, 38].

Figure 7 illustrates the sliding velocity effects on the coefficient of friction of composites made of Gr-reinforced Zinc-Aluminum alloys. The coefficient of friction (COF) increases with increasing sliding velocity and decreases with increasing graphite content. It was discovered that, when compared to the specified weight percentage of the composite, the 0 wt.% Gr-reinforced Zinc-Aluminum alloy composite exhibits the highest value of (μ), which is 0.93 at the value of 1.78 m/s of sliding velocity. According to the figure, the 6 wt.% Gr-ZA-27 produced composite has the lowest coefficient of friction (μ), in the group. This could be explained by the potential that the unyielding action of the cutting tool increases the coefficient of friction (COF), which, if it happens, can harm the material’s surface over deep grooves or scratches. The material deformation between the flat specimen and spinning disc may also be a contributing factor to the higher coefficient of friction. The greatest material loss is produced at the highest sliding velocity and highest friction. [12, 39].

Figure 8 shows the impact of altering the normal load (10–40) N on the specific wear rate of Gr-filled Zinc-Aluminum alloy composites under a constant test condition (slide distance = 700 m; sliding speed = 1 m/s). It was found that adding graphite causes the specific wear rate of specified Gr-ZA-27 alloy composites to decrease while increasing applied load. It forms a thin layer of graphite coating on the upper section of the counter surfaces, stopping sub-surface contact during sliding, when employed as a solid lubricant in sliding tests. The order of the specified wear rates is

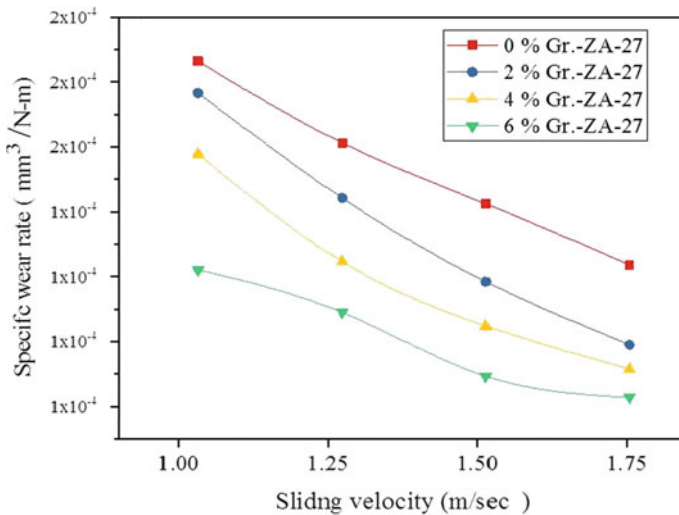


Fig. 6 Effect of sliding velocity on the specific wear rate of alloy composite

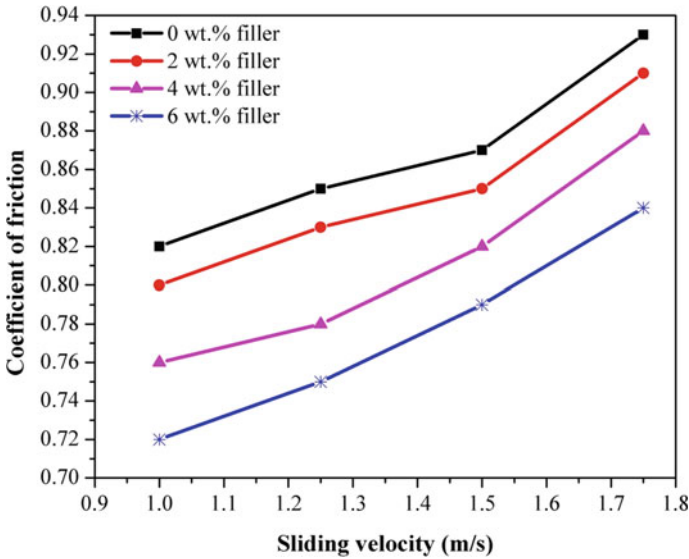


Fig. 7 Effect of sliding velocity on the coefficient of friction of alloy composite

0 wt.% GR-ZA27 > 2 wt.% GR-ZA27 > 4 wt.% GR-ZA27 > 6 wt.% GR-ZA27. The Zinc-Aluminum matrix and graphite content, which exhibit strong adhesion bonding conditions between the matrix and filler content, may be responsible for the good wear performance of 6 wt.% GR-ZA27 alloy composite. Due to the high porosity, the hardness of the manufactured alloy composite diminishes, which accounts for the rise in the alloy composite’s specific wear rate as the normal load is increased. Numerous scientists and researchers have reported findings that are similar [41, 42].

The influence of the variation of the normal load (10–40) N on COF(μ) of Gr-filled Zinc-aluminum composites is shown in Fig. 9. It is clear that the value of the (COF) rises as the normal load rises; this indicates that the trend of the COF value remains consistent between 10 and 20 N of applied load at the various weight percentages of filler content. The COF value then increased in the load range (30–40) N, rising from roughly 0.29 to 0.31 for the 0 wt.% of Gr-filled ZA-27 alloy composite, indicating that it has the best values when compared to the other alloy composites that were investigated. The planned alloy composite’s COF order is as follows: 0 wt.% Gr-ZA-27 > 2 wt.% Gr-ZA-27 > 4 wt.% Gr-ZA-27 > 6 wt.% Gr-ZA-27. This may be caused by the emergence of a mechanical layer and the sliding disintegration of asperities debris particles. With increasing applied load, it is seen that the alloy composites with 6 wt% Gr-filled Zinc-aluminum (ZA-27) exhibit the lowest friction. This is caused by a variety of wear mechanisms and thermal softening beneath the worn-out surface as a result of temperature rise [4]. It should be noticed that this specially constructed composite minimizes the friction coefficient of the composite and minimizes contact between the pin and the disc. This leads to the conclusion that adding graphite content to unfilled alloy enhances wear behaviour, engineered

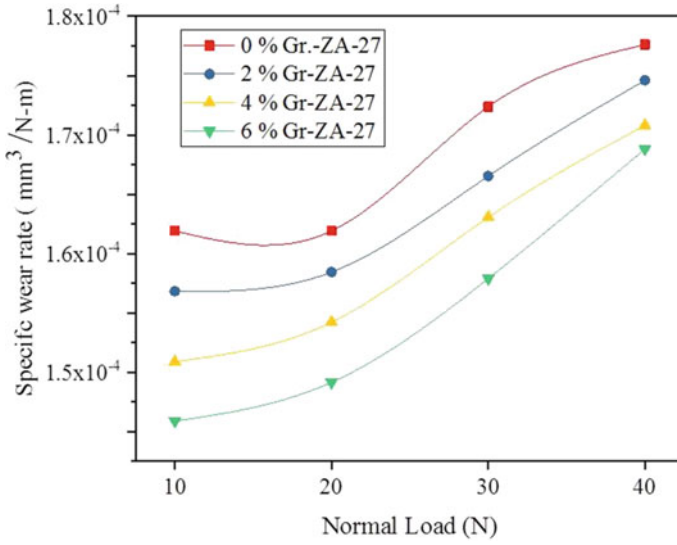


Fig. 8 Effect of normal load on the specific wear rate of alloy composite

composites perform considerably better than matrix alloy, and wear and friction coefficients fall as graphite content is increased [35].

Figure 10 shows the effect of sliding distance of a Gr-reinforced ZA-27 alloy composite on the specific wear rate. It has been found that as sliding distance increases, the specific wear rate of specified composites also increases. It's possible that an increase in reaction time and disc rotation leads to an increase in the sliding surface contact area, which in turn increases the specific wear rate. The following

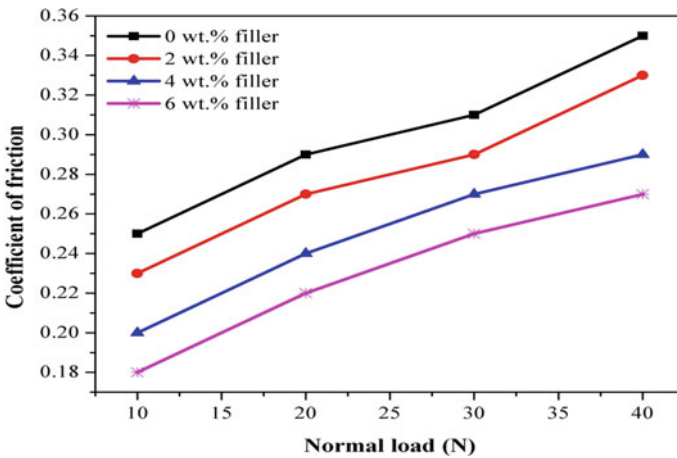


Fig. 9 Effect of normal load on the coefficient of friction of alloy composite

is the order of the specific wear rate: 0 wt. % Gr-ZA-27 > 2 wt.% Gr-ZA-27 > 4 wt.% Gr-ZA-27 > 6 wt.% Gr-ZA-27. It was evident from the graph that the specific wear rate of the composite was the smallest at a sliding distance of just 700 m, and it increases in the whole range. In comparison to specified alloy composites, the specific wear rate of the unfilled alloy composite is often higher. Because the sliding disk's bottom section is steady, the particles are broken, and exhausted debris particles pass through the counter surface.

The effect of increasing sliding distance (700–2800) m on COF (μ) of Gr-filled Zinc-aluminum (ZA-27) alloy composites is shown in Fig. 11. The COF(μ) value decreases when the alloy composite's Gr (0–6% wt%) content is increased. The COF value of the designed composite displays the higher at 0 weight per cent. At 2 wt.% Gr powder reinforced ZA-27 alloy composite, COF value was reduced. However, the decline in wear rate trend indicates damage to the alloy composite and reduction in the micrograph structure. Specific grain sizes, and grain shape distribution are also supportive of wear attributes. It was found that for alloy composite, the COF magnitude was smaller at a lower sliding distance. With increasing sliding distance for the Gr-filled Zinc-Aluminum alloy composite, the COF of the material gradually improves. This may be due to grain expansion and an increase in hardness [12, 43].

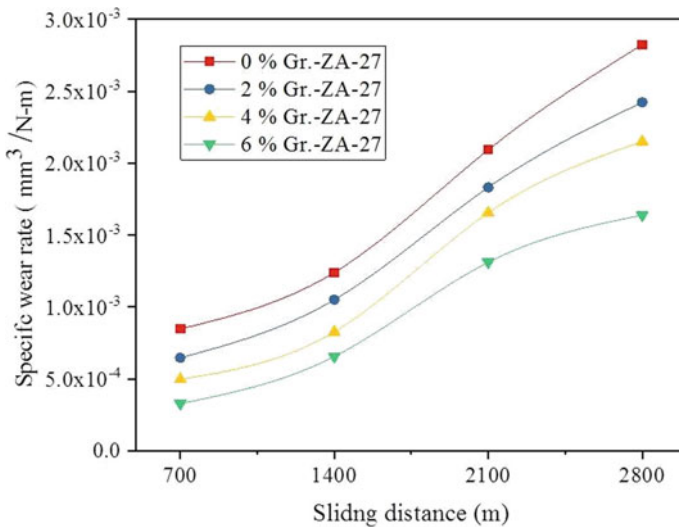


Fig. 10 Effect of the sliding distance on the specific wear rate

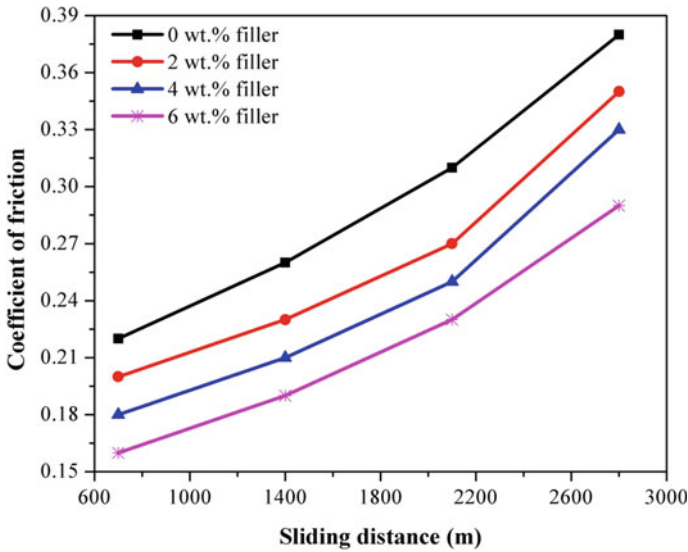
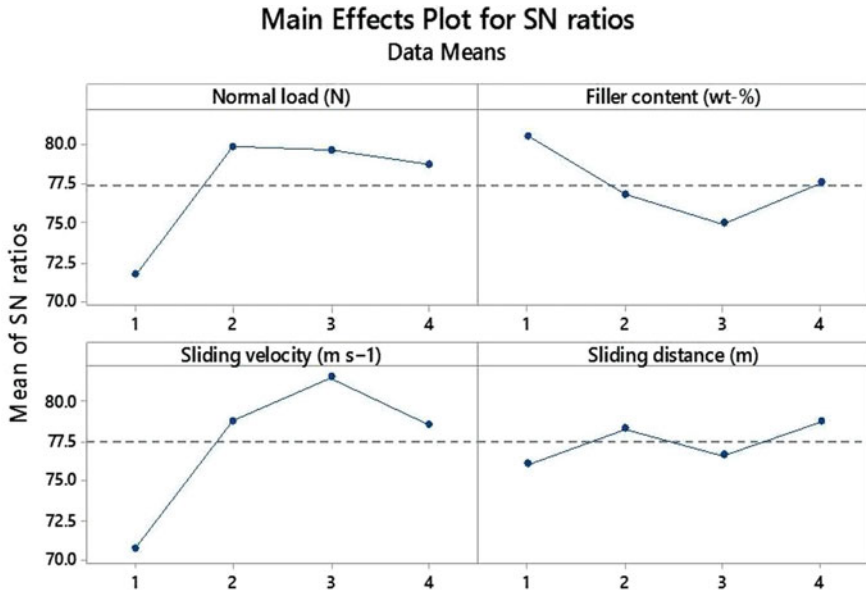


Fig. 11 Effect of the sliding distance on the coefficient of friction

3.3 Analysis of Experimental Results by Taguchi Experimental Design

The robustness and signal-to-noise (S/N) ratio is estimated using the Taguchi method, which is a very useful part of a parametric design. In this strategy, the words “signal” and “noise” refer to the desired outcome, which in this case is wear rate, and the unwanted background, respectively. The values for the S/N ratio shown in Table 2 are the average of two replications. The composites that were created and filled with graphite have an overall mean S/N ratio of 75.25 dB. The MINITAB 14 programme is used to analyse the Taguchi data. Before using this model as a forecast for performance estimation, any test must take into account the proper interactions between the control parameters. However, a composite factorial design was used to measure the interaction impact.

Figure 12 shows how control factors affect wear rate in the appropriate ways. The order of importance of the control parameters for composites, from normal load (L) to reinforcement or filler content (R), to sliding velocity (V), to sliding distance (SD) [44, 45], is given below.



Signal-to-noise: Smaller is better

Fig. 12 Influence of control parameters on signal-to-noise ratio (S/N)

3.4 Analysis of Variance (ANOVA) and Effect of Control Parameters

The wear rate of the composite was the control parameter that was observed using ANOVA, along with its percentage share in the calculation of the response. The research was done using 5% (level of significance). Normal load (41.81%), reinforcement or filler content (22.98%), sliding velocity (14.55%) and sliding distance (11.53%) are the results of the ANOVA, in that order (see Table 3). The order of key control parameters demonstrates their ability to fully regulate the wear system’s whole mechanism.

3.5 Surface Morphology

Graphite-reinforced Zinc aluminium (ZA-27) alloy composite SEM micrographs for sliding wear (stationary state condition; Taguchi DOE; L16 orthogonal array) at varied load (10–40) N are shown in Fig. 13(a-d). Due to the lowest stress (10 N) and slowest sliding speed (1 m/sec), delaminations are seen in the SEM picture of the sample (0 wt.% Gr-ZA-27 Gr) in Fig. 13a. The delamination may result from insufficient frictional heating of the counter face and substantial material removal

Table 3 Wear rate of response of ANOVA table for S/N ratios

Source	DF	Seq SS	Adj SS	Adj MS	F	P	P (%)
Normal load (L)	4	1300.72	1226.63	340.46	7.87	0.019	41.81
Filler content (F)	4	651.06	648.73	120.86	5.08	0.188	22.98
Sliding velocity (V)	4	641.13	685.85	187.52	6.67	0.115	14.55
Sliding distance (D)	4	2472.72	1462.89	362.48	8.19	0.016	11.53
Error	8	504.33	534.35	64.47			15
total	24	5569.96					100

Standard deviation (S) = 8.24402 R^2 (R-Sq) = 90.54% Adjusted R^2 (R-Sq (adj)) = 80.93% (DF = Degrees of freedom, Seq SS = Sequential sums of squares, Adj SS = Adjusted sums of squares, Adj MS = Adjusted mean squares, F = Variance, P = Probability)

from the sample surface, and it happens at low load and slow sliding velocity [43]. Shallow grooves can be seen on the surface of the sample (2 wt% Gr-ZA-27 Gr) in the SEM image of the sample in Fig. 13b under a normal load of 20 N. In steady state sliding tests, heat is produced at the interface of the materials' surfaces when the two flat pieces are rubbed together because of friction. As a result of the surface's mellowing, wear particles are impaired and shallow composite grooves develop [46]. The SEM picture of the sample (4 wt.% Gr-ZA-27 Gr) with a normal load of 30 N is shown in Fig. 13c. Debris particles (PD) can be seen on the worn-out surface when using an increase in load. This is due to the fact that friction at the interface generates heat, which causes the wear particles to degrade and the surface to mellow [47]. The ploughing mechanism is generated due to the highest content of plastic deformation, as can be seen in the SEM micrograph of sample (6 wt% Gr-ZA-27 Gr) for sliding wear with normal load 40 N in Fig. 13d. Numerous researchers [48–55] obtained similar results.

3.6 Ranking Optimization Using PSI Method

In this research chapter, the PSI method is used to analyse the decision matrix (D), which has four composite specimens (AGR0, AGR2, AGR4 and AGR6) as alternatives and performance criteria that are provided in Table 4. The following are the step-by-step calculations:

Step 1: The evaluated performance data are organized in the form of decision matrix shown in Table 5.

Step 2: The decision matrix has been normalized as per the algorithm, as shown in Table 6.

Step 3–7: Table 7 displays the final ranking order of alloy composites determined using the technique along with the intermediate calculations.

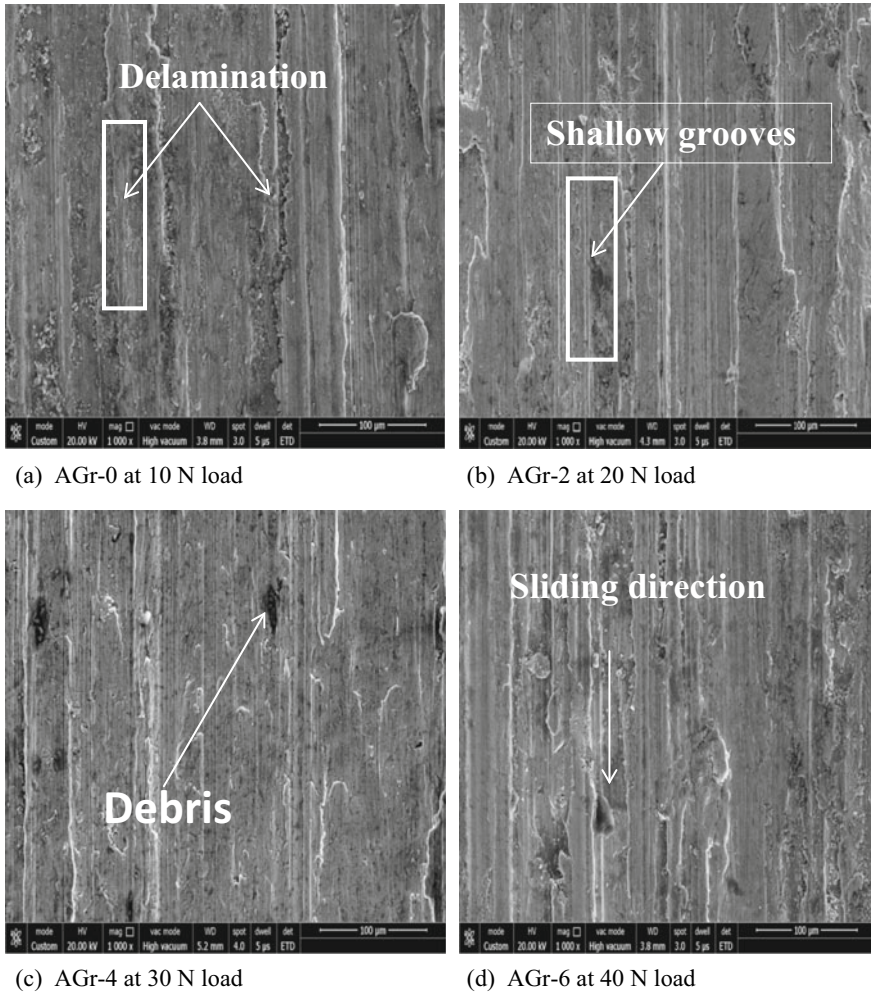


Fig. 13 SEM micrographs of graphite-reinforced ZA-27 alloy composite samples for sliding wear at varying load (10–40) N

4 Conclusions

High vacuum casting was used to create the alloy composite ZA-27-GR. UTM and multi-specimen tester machines were used to analyse the mechanical and tribological characteristics of alloy composites made of ZA-27-GR. PSI Method was used to analyse the ranking order.

The following points serve as the conclusion:

1. The physical and mechanical characterization like (Voids content (VC); Hardness (H); Impact strength (IM); Flexural strength (FS); Density (D)) of

Table 4 Descriptions of the selection criteria applied in this case study

Sr. no	Performance criteria	Preference
1	Tensile strength (MPa)	Maximum
2	Flexural strength (MPa)	Maximum
3	Impact strength (J)	Maximum
4	Hardness (HRB)	Maximum
5	Compressive strength	Maximum
6	Density (g/cc)	Minimum
7	Void content (%)	Minimum
8	Specific wear rate (mm ³ /Nm)	Minimum
9	COF	Minimum

Table 5 Decision matrix

	Material alternatives	0%	2%	4%	6%
PC's	Property ↓				
PC-1	Tensile strength (MPa)	290	340	395	428
PC-2	Flexural strength (MPa)	300	363	342	490
PC-3	Impact strength (J)	22.76	33.5	58.5	64
PC-4	Hardness (HRB)	107	135	151	171
PC-5	Compression strength (MPa)	406	420	450	496
PC-6	Experimental density (g/cc)	4.55	4.57	4.5	4.42
PC-7	Voids content (%)	2.53	3.26	4.36	1.36
PC-8	Specific wear rate at sliding distance (mm ³ /Nm)	2.8	2.5	1.8	1.4
PC-9	Coefficient of friction at sliding distance	0.19	0.28	0.35	0.55

Table 6 Normalization of the decision matrix

Material Alternatives → PC's ↓	0%	2%	4%	6%	Mean
PC-1	0.67	0.78	0.91	1.00	0.84
PC-2	1.00	0.87	0.82	0.65	0.83
PC-3	1.00	0.91	0.78	0.62	0.82
PC-4	1.00	0.95	0.88	0.76	0.90
PC-5	0.82	0.85	0.91	1.00	0.89
PC-6	0.97	0.97	0.98	1.00	0.98
PC-7	0.54	0.42	0.31	1.00	0.57
PC-8	0.50	0.56	0.78	1.00	0.71
PC-9	1.00	0.68	0.54	0.35	0.64

Table 7 Ranking of the composites

Material alternatives	0%	2%	4%	6%
PC's ↓				
PC-1	0.0906	0.1050	0.1159	0.0773
PC-2	0.1009	0.0946	0.0757	0.1161
PC-3	0.1030	0.0879	0.0697	0.1134
PC-4	0.1141	0.1055	0.0913	0.1198
PC-5	0.1028	0.1101	0.1214	0.994
PC-6	0.1196	0.1215	0.1237	0.1202
PC-7	0.0374	0.0280	0.0896	0.0482
PC-8	0.0585	0.0813	0.1046	0.0523
PC-9	0.0649	0.0519	0.0330	0.0956
Preference Selection Index	0.79	0.79	0.82	0.84
Preference ranking	4	3	2	1

composite decrease with increment in Gr (0–6 wt. %) reinforcement, while the Tensile strength and compressive strength of composite shows an increasing in trend.

2. The ZA-27-Gr alloy composites under study with the base alloy at steady state sliding, wear parameters as normal load (10–40 N), sliding velocity (1-1.75 m/s) and sliding distance (700-2800 m) show the predominant wear resistance performance, thus they could be broadly utilized for bearing material application.
3. The specific wear rate of ZA-27-Gr alloy composites decreases with the increase in sliding velocity (1–1.75 m/s) under the steady state wear test irrespective of the reinforcement. The wear rate order is (0 wt.% Gr –ZA-27 > 2 wt.%Gr-ZA-27 > 4 wt.%Gr-ZA-27 > 6 wt.% Gr-ZA-27). Also, the coefficient of friction increases with the increase in filler content with the order: 0 wt.% Gr-ZA-27 > 2 wt.% Gr-ZA-27 > 4 wt. % Gr-ZA-27 > 6 wt. % Gr-ZA-27 across the entire sliding velocity range.
4. Specific wear rates of Gr-reinforced ZA-27 alloy composite decrease with increasing the normal load (10–40 N) under the steady state wear test. The specific wear rate order is: 0 wt.% Gr –ZA-27 > 2 wt.% Gr-ZA-27 > 4 wt.% Gr-ZA-27 > 6 wt.% Gr-ZA-27. Also, the coefficient of friction decreases with increasing filler content with the order : 0 wt.% Gr-ZA-27 > 2 wt.% Gr-ZA-27 > 4 wt.% Gr-ZA-27 > 6 wt.% Gr-ZA-27 across the entire range of the normal load.
5. Under the steady state wear test, the specific wear rates of Gr-reinforced ZA-27 alloy composite rise with increasing sliding distance (700–280 m), regardless of the reinforcement. Additionally, as filler content increases, the coefficient of friction falls in the following order: 0 wt.% Gr-ZA-27 > 2 wt.% Gr-ZA-27 > 4 wt.% Gr-ZA-27 > 6 wt.% SiC-Gr-ZA-27 across the entire range of sliding distance.

6. Using the design of experiment (DOE) Taguchi approach, the total average for (S/N) proportions for specific wear rate of composites was determined to be 75.25 db. Normal load > filler content > sliding velocity > sliding distance is the whole hierarchy of the critical factors affecting the reduction of wear rate. At a 5% significance level, the ANOVA method is used to corroborate the same results.
7. The priority order of performance criteria is as follows: Tensile Strength (TS) ~ Flexural Strength (FS) ~ (ImpactStrength) ~ (Compressive Strength) ~ Hardness (HVR) > Density (D) > Voids Content (VC) > Wear (W) ~ Coefficient Of Friction.
8. The PSI technique assigns the highest ranking to the alloy composites that have been manufactured and have a uniformly mixed base alloy and particle reinforcement because of their superior qualities. The analysis of performance by PSI method depicted the ranking order AGR6 > AGR4 > AGR2 > AGR0.
9. The PSI approach can be utilized to successfully develop a better composite formulation composition when there are conflicting performance objectives.
10. The analysis of wear data and SEM micrographs of composites made of 6 wt.% Gr-ZA-27 alloy demonstrates their superior wear performance when compared to other composites, making them suitable for use as tribological applications.

Acknowledgements The authors express their truthful gratitude to the Department of Mechanical Engineering of MNITJaipur-302017, Rajasthan, INDIA for their all kinds of financial as well also the miscellaneous infrastructural support. In addition, the authors thank the Institute's Advanced Research Lab for Tribology and Material Research Centre for their assistance and facilities with the experimental and characterization work.

References

1. S.S. Owoeye, D.O. Folorunso, B. Oji, S.G. Borisade, *Int. J. Adv. Manuf. Tech.* **170**, 760 (2018)
2. S.C. Tjong, Z.Y. Ma, *Mater. Sci. Eng.* **29**, 49 (2000)
3. S.A.B. Raju, K.C. Hemanth, S.I.N. Jayasimha, *Proc. Int. Conf. Eng. Sci. Tech. ICCTEST - 2017*, 228–232s, (2017)
4. R. Dalmis, H. Cuvalci, A. Canakci, O. Guler, *Adv. Compos. Lett.* **25**(2), 37 (2016)
5. G. Ranganath, S.C. Sharma, M. Krishna, *Wear* **251**, 1408 (2001)
6. S.C. Sharma, K.H.W. Seah, B.M. Satish, B.M. Girish, *Mater. Des.* **17**(6), 245 (1996)
7. K.K. Alaneme, K.O. Adeoye, S.K. Oke, *Leon. Electro. J.* **29**, 1 (2016)
8. B.M. Girisha, K.R. Prakash, B.M. Satisha, *Mater. Sci. Eng. A.* **530**, 382 (2011)
9. A. Baradiswaran, A.E. Perumal, *Int. J. Compos. Part B.* **54**, 146 (2013)
10. A. Kumar, M. Kumar, *Mater. Today Proc.* **27**, 2617 (2019)
11. A. Kumar, M. Kumar, *Mater. Today. Proc.* **27**, 2667 (2019)
12. A. Kumar, A. Patnaik, I.K. Bhat, *J. Powder Metallur.* **60**, 371 (2017)
13. A. Kumar, M. Kumar, B. Pandey, *SILICON* **14**(5), 2051 (2022)
14. M. Kumar, S. Bhashkar, N.K. Shakyawal, A. Kumar, *Materialwiss. Werkstofftech.* **51**, 1662 (2020)
15. A. Kumar, V. Kukshal, V.R. Kiragi, *Mater. Today Proc.* **44**, 4349 (2021)
16. A. Kumar, V. Kumar, A. Kumar, B. Nahak, R. Singh, *Mater. Today. Proc.* **44**, 4542 (2021)

17. A. Kumar, M. Kumar, A. Patnaik, M.J. Pauer, A. Pandey, A. Kumar, V. Gautam, *Mater. Today Proc.* **44**, 4784 (2021)
18. M.A. Maleque, S. Dyuti, M.M. Rahman, *Proc. Worl. Congr. Eng.* **1**, 2078 (2010)
19. K. Maniya, M.G. Bhatt, *Mater. Des.* **31**, 1785 (2010)
20. M. Kumar, A. Kumar, *Mater. Today Proc.* **27**, 20120 (1972)
21. B.D. Agarwal, L.J. Broutman, in *Analysis and Performance of Fiber Composites*, 2nd edn. (Jhon. Wiley Sons, 1990), pp. 440–442
22. R. Kumar, K. Kiran, V.S. Sreebalaji, *Measure.* **102**, 142 (2017)
23. S.S. Kumar, M. Devaiah, *Ceram. Int.* **38**, 1139 (2012)
24. S. Gangwar, A. Patnaik, I.K. Bhat, *SILICON* **8**, 601 (2016)
25. D. Petkovic, M. Madic, M. Radovanovic, V. Gecevska, *Facta. Univ. Ser. Mech. Eng.* **15**, 97 (2017)
26. R. Attri, S. Grover, J. King, *Saud. Univ. Eng. Sci.* **27**, 207 (2015)
27. K. Jha, S. Chamoli, Y.K. Tyagi, H.O. Maurya, *Mater. Today Proc.* **5**, 3353 (2018)
28. R. Khorshidi, A. Hassani, *Mater. Des.* **52**, 999 (2013)
29. M. Panahi, H. Gitinavard, *J. Sustain. Min.* **16**, 207 (2018)
30. K. Mesran, R.D. Tampubolon, R.D. Sianturi, F.T. Waruwu, *Sci. Tech.* **3**, 230 (2017)
31. S.Y. Jian, S.J. Tao, X.R. Huang, *Adv. Mater. Res.* **1078**, 290 (2014)
32. H. Abdizadeh, R. Ebrahimifard, M.A. Baghchesara, *Compos. Part B.* **56**, 217 (2014)
33. X. Li, C. Guo, X. Liu, *Prog Nat Sci.* **24**, 478 (2014)
34. S.C. Sharma, B.M. Girish, R. Kamath, B.M. Satis, *Wear* **219**, 162 (1998)
35. T. Rajmohan, K. Palanikumar, S. Ranganathan, *Trans. Nonferrous Met. Soc.* **23**, 2509 (2013)
36. A. Baradeswaran, A.E. Perumal, *Compos. Part B.* **56**, 472 (2014)
37. B.V. Ramnath, C. Elanchezian, M. Jaivignesh, *Mater. Desi.* **58**, 332 (2014)
38. S. Ozden, R. Ekici, N. Nair, *Compos A Appl S.* **38**, 484 (2007)
39. J.U. Ejjioforand, R.G. Reddy, *J. Miner. Proc.* **49**, 31 (1997)
40. B.P. Krishanand, P.K. Rohatgi, *Meter. Technol.* **11**, 41 (1984)
41. L.I. Xuan, G. Chao, L. Xiaokai, *Mater. Int.* **24**, 472 (2014)
42. S. Baskaran, V. Anandakrishnan, M. Duraiselvam, *Mater. Des.* **60**, 184 (2014)
43. A.K. Mondal, S. Kumar, *Wear* **267**, 458 (2009)
44. H. Chi, L. Jiang, G. Chen, *Mater. Des.* **87**, 960 (2015)
45. K. Nirajan, P.R. Lakshminarayanan, *Mater. Des.* **47**, 167 (2015)
46. S.A. Alidokhta, A.A. Zadeh, H. Assadi, *Wear* **305**, 291 (2013)
47. H.R. Manohara, T.M. Chandrashekharaiah, K. Venkateswarlu, S.A. Kori, *Tribol. Int.* **51**, 54 (2012)
48. C.S. Ramesh, R. Keshavamurthy, B.H. Channabasappa, *Tribol. Int.* **43**, 623 (2010)
49. J.C. Walker, W.M. Rain, H. Jones, *Wear* **259**, 577 (2005)
50. E. Naveena, S. Ilangovan, *Mater. Today: Proc.* **22**, 2704 (2020)
51. O. Savas, *Mater. Today Communi.* **23**, 100 (2020)
52. T. Sathis, S. Karthick, *J. Mater. Sci. Technol.* **9**(3), 3481 (2020)
53. S. Arif, B. Jamil, M. Sheikh, *Engg. Sci. Tech. Int. J.* **23**, 674 (2020)
54. X. Li, M. Sosa, U. Olofesson, *Wear* **340**, 31 (2015)
55. T.S. Kran, M.P. Kumar, S. Basarajappa, B.M. Viswanatha, *Mater. Des.* **63**, 294 (2014)